U(1) × U(1) symmetry-protected topological order in Gutzwiller wave functions

Citation: Liu, Zheng-Xin, Jia-Wei Mei, Peng Ye, and Xiao-Gang Wen. "U(1) × U(1) symmetry-protected topological order in Gutzwiller wave functions." Phys. Rev. B 90, 235146 (December 2014). © 2014 American Physical Society

As Published: http://dx.doi.org/10.1103/PhysRevB.90.235146

Publisher: American Physical Society

Persistent URL: http://hdl.handle.net/1721.1/92722

Version: Final published version: final published article, as it appeared in a journal, conference proceedings, or other formally published context

$U(1) \times U(1)$ symmetry-protected topological order in Gutzwiller wave functions

Zheng-Xin Liu,[1,2] Jia-Wei Mei,[2] Peng Ye,[2] and Xiao-Gang Wen[3,2,1]

[1]*Institute for Advanced Study, Tsinghua University, Beijing 100084, People's Republic of China*

[2]*Perimeter Institute for Theoretical Physics, Waterloo, Ontario, Canada N2L 2Y5*

[3]*Department of Physics, Massachusetts Institute of Technology, Cambridge, Massachusetts 02139, USA*

(Received 7 September 2014; revised manuscript received 8 December 2014; published 24 December 2014)

Gutzwiller projection is a way to construct many-body wave functions that could carry topological order or symmetry-protected topological (SPT) order. However, an important issue is to determine whether or not a given Gutzwiller-projected wave function (GWF) carries a nontrivial SPT order, and which SPT order is carried by the wave function. In this paper, we numerically study the SPT order in a spin $S = 1$ GWF on the kagome lattice. Using the standard Monte Carlo method, we directly confirm that the GWF has (1) gapped bulk with short-range correlations, (2) a trivial topological order via a nondegenerate ground state, and zero topological entanglement entropy, (3) a nontrivial $U(1) \times U(1)$ SPT order via the Hall conductances of the protecting $U(1) \times U(1)$ symmetry, and (4) a symmetry-protected gapless boundary. This represents numerical evidence of continuous symmetry-protected topological order in two-dimensional bosonic lattice systems.

DOI: 10.1103/PhysRevB.90.235146 PACS number(s): 73.43.−f, 11.15.Yc, 87.55.K−

I. INTRODUCTION

Topological order [1–3] was introduced to describe exotic quantum phases without symmetry breaking, such as fractional quantum Hall states [4,5] or spin-liquid states [6,7]. Opposite to Landau's paradigm of symmetry-breaking orders [8,9], topologically ordered phases cannot be distinguished by local order parameters. It was shown that different topological orders differ by many-body entanglement [10]. From this point of view, long-range entangled states are topologically ordered and are characterized by exotic properties, such as degeneracy of ground states on a torus, fractional excitations, and nonzero topological entanglement entropy [11,12]. On the other hand, a short-range entangled state is trivial and can be adiabatically connected to a direct product state. However, if the system has a symmetry, the phase diagram will be enriched. Even short-range entangled states can belong to different phases, called symmetry-protected topological (SPT) phases [13,14]. The Haldane phase [15,16] and topological insulators [17–21] are typical examples of phases that contain SPT orders. If the symmetry of a bosonic system is described by group G, then a large class of SPT phases in $d + 1$ dimension can be constructed via group cohomology $\mathcal{H}^{d+1}(G, U(1))$ [22] or through nonlinear σ models [22,23]. In 2+1 dimensions (D), many SPT phases can also be understood through Chern-Simons effective theory [24]. Similar to quantum Hall states and topological insulators, the boundary of a 2+1D SPT phase must by gapless if the symmetry is not broken. For continuous symmetry groups such as $U(1)$ [22,24–27] or $SO(3)$ [28], different SPT phases can be distinguished by Hall conductance, which are quantized to 2. We would like to remark that before the recent studies of symmetry-protected short-range entangled states with trivial topological order (i.e., the SPT states), some progress was made on symmetry-enriched long-range entangled states with nontrivial topological order, i.e., the so-called symmetry-enriched topological states [29–34], where the "fractionalized representation" of the symmetry, carried by topological excitations and described by projective symmetry group [29–31], played a key role.

Although it is believed that symmetry can enrich quantum phases of matter, it lacks simple lattice models to realize these nontrivial phases in a spatial dimension higher than 1+1D. SPT phases for discrete symmetry groups were understood quite well, since the ground-state wave functions and exactly solvable models (which are usually complicated and contain many-body interactions) for nontrivial SPT phases can be constructed [35,36]. It is more challenging to realize continuous symmetry-protected phases. A $U(1)$ symmetry-protected nontrivial phase was reported in a continuous Bose model [27], and lattice models that may realize continuous (or combined) symmetry-protected topological phases were proposed [37–40]. In Ref. [38], the authors proposed projective construction of $SU(2)$ or $SO(3)$ SPT states. And lattice model Hamiltonians that may possibly stabilize SPT states with continuous symmetries were recently designed [39–41].

Using Gutzwiller-projected wave functions (GWF), we can construct different kinds of SPT states. In the present paper, we will numerically study a spin-1 state on the kagome lattice constructed by Gutzwiller-projected Chern bands, which was proposed in Ref. [37]. We will show that this state is a $U(1) \times U(1)$ SPT state, where the two $U(1)$ groups correspond to $\sum S_{z,i}$ conservation and $\sum S_{z,i}^2$ conservation, respectively. This SPT state has the following properties: it is gapped without conventional long-range spin order; it has unique ground-state and zero topological entanglement entropy; it has nonzero spin Hall conductance, the $U(1) \times U(1)$ charge is not fractionalized; and the boundary is gapless if the symmetry is reserved but can be gapped out by the perturbations that break the symmetry. As a comparison, we also study a $S = 1$ chiral spin-liquid state [42] which is long-range entangled and contains intrinsic topological order, and show that its gapless edge state is robust against symmetry-breaking perturbations. These properties of the Gutzwiller wave functions are directly confirmed numerically using the standard Monte Carlo method.

Remarkably, before projection, the above two states are both chiral at the mean-field level, but after projection the SPT state becomes nonchiral and the chiral spin liquid remains chiral.

The remaining part of this paper is organized as follows. In Secs. II and III, we briefly review the parton construction of Gutzwiller-projected wave functions, and introduce their

low-energy effective-field theory under two different approximations. Readers who are only interested in numerical results may go directly to Sec. IV, where we show that the GWF we are studying has (1) gapped short-range correlation in the bulk, (2) zero topological entanglement entropy and a unique ground state, (3) nontrivial Hall conductance, and (4) a symmetry-protected gapless boundary. Section V is devoted to a summary.

II. MEAN-FIELD THEORY OF PARTON CONSTRUCTION AND ITS EFFECTIVE-FIELD THEORY

There are two approximations to calculate the low-energy effective theory from the parton construction: the mean-field approach and the Gutzwiller-projection approach. They represent two different approximations. The mean-field approach is simple, but for some systems it captures the main physical picture given that the mean-field parameters are chosen properly. The disadvantage is that the Hilbert space has been enlarged and local quantum fluctuations are neglected. To obtain better results, one needs to go beyond the mean-field approximation and couple the partons to internal gauge fields. This problem is partially solved in the Gutzwiller approach, where the mean-field states are projected onto the original Hilbert space. In this section, we will introduce the mean-field approach of the parton construction, while the Gutzwiller-projection approach will be introduced in Sec. III.

A. Parton construction

We adopt the fermionic representation (see the review paper [43], and references therein) of spin operators $\hat{S}_i^\alpha = F_i^\dagger \mathcal{S}^\alpha F_i$ with $\alpha = x,y,z$. In the case of $S = 1$, $F_i = (f_{1i}, f_{0i}, f_{-1i})^T$, $\mathcal{S}^\alpha$ are 3×3 matrices, and the three spin bases are represented as $|m\rangle = f_m^\dagger|\text{vac}\rangle$ with $m = 1,0,-1$ [44–47]. Here a particle-number constraint $\hat{N}_i = f_{1i}^\dagger f_{1i} + f_{0i}^\dagger f_{0i} + f_{-1i}^\dagger f_{-1i} = 1$ should be imposed to ensure that the Hilbert space of fermions is the same as that of the spin. Notice that the spin operator is invariant under the following $U(1)$ gauge transformation $F_i \to F_i e^{i\varphi_i}$.

From the fermionic representation of $S = 1$ spin operators, we will consider the following pairing-free mean-field Hamiltonian on the kagome lattice [37]:

$$H_{\text{mf}} = \sum_{ij}(t_{m,ij} e^{i\tilde{a}_{ij}} f_{m,i}^\dagger f_{m,j} + \text{H.c.}) + \sum_i \lambda_i(\hat{N}_i - 1), \qquad (1)$$

where the complex hopping coefficient $t_{m,ij}$ can be considered as Hubbard-Stratonovich fields in path-integral language, and the averaged value $\lambda_i = \bar{\lambda}$ is the chemical potential. Since the fermionic representation has a $U(1)$ gauge structure, the mean-field state suffers from gauge fluctuations. Here $(\tilde{a}_{ij}, \lambda_i)$ are the space and time components of the internal $U(1)$ gauge field $\tilde{a}_\mu$, corresponding to the phase fluctuations of $t_{m,ij}$ and the fluctuation of $\bar{\lambda}$, respectively. We integrate out $\tilde{a}_\mu$ to project into the physical Hilbert space. In the mean-field approximation, $(\tilde{a}_{ij}, \lambda_i)$ are not integrated out and will be fixed as $(\tilde{a}_{ij}, \lambda_i) = (\bar{a}_{ij}, \bar{\lambda})$.

By tuning the phase of $t_{m,ij}$, we can set the Chern number of each species of fermions to be either 1 or -1. For example, if we only consider nearest-neighbor hopping and set the phase to be $e^{\pm i\pi/6}$ [see Figs. 1(a) and 1(a)], then the Chern number for the lowest band is ± 1. In the following discussion, we will use the notation $|\mathcal{C}_1\mathcal{C}_0\mathcal{C}_{-1}\rangle$ to denote the mean-field state, where the number $\mathcal{C}_m = \pm 1$ stands for the Chern number of the f_m species of fermion.

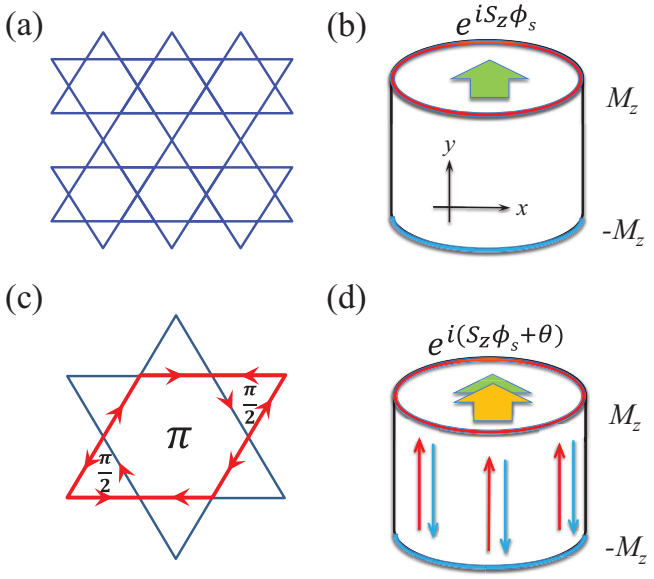

FIG. 1. (Color online) (a) The kagome lattice. (b) Laughlin's gauge-invariant argument of the spin Hall conductance. The insertion of a symmetry flux through the cylinder results in symmetry charge pumping from one edge to the other [M_z stands for $\sum S_{z,i}$ momentum according to the first $U(1)$ symmetry. Similarly, for the second $U(1)$ symmetry, the inserted flux should be $e^{iS_z^2\phi_s}$ and then M_z stands for $\sum S_{z,i}^2$ momentum]. (c) The mean-field model on a kagome lattice with Chern number $\mathcal{C} = 1$. When hopping along the arrows, the fermion gains a phase $e^{i\pi/6}$; when hopping against the arrow, the fermion gains a phase $e^{-i\pi/6}$. (d) Laughlin's argument at the mean-field level. An internal gauge flux θ should be introduced such that the induced particle-number flow from one edge to the other exactly cancels that caused by the symmetry flux.

In above mean-field Hamiltonian, the particle numbers of three species of fermions are conserved, respectively. This gives rise to three $U(1)$ spin symmetries. However, if the particle-number constraint is strictly satisfied, then the total charge (namely, the "electric charge") degrees of freedom will be frozen. As a consequence, there are two independent $U(1)$ symmetries for the spin model: one generated by $\sum_i S_{z,i}$ and another by $\sum_i (S_{z,i})^2$. In other words, the symmetry group for the spin system is $U(1)\times U(1)$. To describe the spin system correctly, we should couple the fermions to the internal gauge field $\tilde{a}_\mu$. In the following, we will give the low-energy effective-field theory based on the mean field with fluctuating internal gauge fields.

B. Chern-Simons theory and physical response

Under hydrodynamic and mean-field approximations, we can introduce three Chern-Simons field a_m to describe the current of the three species of fermions via $J_\mu^m = \frac{1}{2\pi}\varepsilon^{\mu\nu\lambda}\partial_\nu a_{m,\lambda}$. Then the mean-field theory can be described by the

Chern-Simons Lagrangian,

$$\mathcal{L}_{\rm MF} = -\frac{i}{4\pi}\sum_m \mathcal{C}_m^{-1}\varepsilon^{\mu\nu\lambda}a_{m,\mu}\partial_\nu a_{m,\lambda},$$

if we set $\tilde{a}_\mu = \text{const}$.

After including fluctuating internal $U(1)$ gauge field $\tilde{a}_\mu$, we obtain the following low-energy effective theory for the spin system:

$$\begin{aligned}\mathcal{L} &= -\frac{i}{4\pi}\sum_m \mathcal{C}_m^{-1}\varepsilon^{\mu\nu\lambda}a_{m\mu}\partial_\nu a_{m\lambda} + \frac{i}{2\pi}\sum_m \varepsilon^{\mu\nu\lambda}\tilde{a}_\mu\partial_\nu a_{m\lambda}\\ &= -\frac{i}{4\pi}\varepsilon^{\mu\nu\lambda}a_\mu^T K\,\partial_\nu a_\lambda, \qquad (2)\end{aligned}$$

where $a_\mu = (a_{1\mu} \quad a_{0\mu} \quad a_{-1\mu} \quad \tilde{a}_\mu)^T$ and

$$K = \begin{pmatrix} \mathcal{C}_1^{-1} & 0 & 0 & 1\\ 0 & \mathcal{C}_0^{-1} & 0 & 1\\ 0 & 0 & \mathcal{C}_{-1}^{-1} & 1\\ 1 & 1 & 1 & 0\end{pmatrix}.$$

We only kept quadratic terms and dropped the Maxwell terms. Since $\tilde{a}_\mu$ can be considered as a Lagrangian multiplier, we can integrate it first and obtain an effective mutual Chern-Simons action described by a 2×2 K matrix (see Appendix C 2) [37].

If $|\det(K)| \neq 1$ (or the signature of K is not zero, where the signature of K is the number of its positive eigenvalues minus the number of negative eigenvalues), then the state of the spin-1 system represented by $|\mathcal{C}_1\mathcal{C}_0\mathcal{C}_{-1}\rangle$ will carry a nontrivial topological order. If $|\det(K)| = 1$ (or the signature of K is zero), then the corresponding spin-1 state will have a trivial topological order. But such a state may have a nontrivial SPT order.

To detect the SPT order, we couple the system with a probe field A_μ^s (according to some symmetry) via

$$\mathcal{L}_{\rm probe} = \frac{i}{2\pi}\varepsilon^{\mu\nu\lambda}A_\mu^s Q^T\partial_\nu a_\lambda,$$

where $Q = [(q^s)^T, 0]^T$, and q^s is the charge carried by the fermions according to the external probe field A_μ^s. For example, for the field $A_\mu^{S_z}$ that couples to the $U(1)$ charge $\sum_i S_i^z$, $q^{S_z} = (1,0,-1)^T$, which gives rise to

$$Q_{S_z} = (1,0,-1,0)^T.$$

For the field $A_\mu^{S_z^2}$ that couples to the $U(1)$ charge $\sum_i (S_i^z)^2$, $q^{S_z^2} = (1,0,1)^T$, which gives rise to

$$Q_{S_z^2} = (1,0,1,0)^T.$$

Integrating out a_μ, we obtain the response theory

$$\mathcal{L}_{\rm res} = \frac{i}{4\pi}\varepsilon^{\mu\nu\lambda}Q^T K^{-1}Q A_\mu^s\partial_\nu A_\lambda^s, \qquad (3)$$

and three Hall conductances,

$$\begin{aligned}\sigma_H^{S_z} &= \frac{1}{2\pi}Q_{S_z}^T K^{-1}Q_{S_z},\\ \sigma_H^{S_z^2} &= \frac{1}{2\pi}Q_{S_z^2}^T K^{-1}Q_{S_z^2}, \qquad (4)\\ \sigma_H^{S_zS_z^2} &= \frac{1}{2\pi}Q_{S_z}^T K^{-1}Q_{S_z^2}.\end{aligned}$$

If one of the above three Hall conductances is nonzero, then the spin-1 state has a nontrivial $U(1)\times U(1)$ SPT order.

C. Response mean-field theory

When the system couples to an external probe field A_μ^s, the mean-field theory should be modified accordingly. To get the correct response mean-field Hamiltonian, we integrate out the matter field $a_{m\mu}$ to obtain the effective Lagrangian,

$$\mathcal{L}_{\rm eff}(A,\tilde{a}) = \frac{i}{4\pi}\sum_m \mathcal{C}_m\varepsilon^{\mu\nu\lambda}(\tilde{a}_\mu + q_m A_\mu^s)\partial_\nu(\tilde{a}_\lambda + q_m A_\lambda^s).$$

The external field A_μ^s will induce a background internal gauge field $\bar{a}_\mu$—the saddle-point value of the $\tilde{a}$ field which can be obtained from $\tilde{J}_\mu = \frac{\delta\mathcal{L}_{\rm eff}(A^s,\tilde{a})}{\delta\tilde{a}_\mu} = 0$ [48] in a proper gauge choice,

$$\bar{a}_\mu = -\frac{\sum_m \mathcal{C}_m q_m}{\sum_m \mathcal{C}_m}A_\mu^s. \qquad (5)$$

Rewriting $\tilde{a}_\mu = \bar{a}_\mu + \delta\tilde{a}_\mu$, we have

$$\mathcal{L}_{\rm eff}(A,\delta\tilde{a}) = \frac{i}{4\pi}\sum_m \varepsilon^{\mu\nu\lambda}\mathcal{C}_m\left[\tilde{q}_m^2 A_\mu^s\partial_\nu A_\lambda^s + \delta\tilde{a}_\mu\partial_\nu\delta\tilde{a}_\lambda\right],$$

where $\tilde{q}_m = q_m(1 - \frac{\sum_n q_n\mathcal{C}_n}{q_m\sum_n\mathcal{C}_n})$ is the screened charge. Integrating out $\delta\tilde{a}_\mu$, we obtain the response Lagrangian and the spin Hall conductance is given by $\sigma_H^s = \frac{1}{2\pi}\sum_m \mathcal{C}_m\tilde{q}_m^2$.

Notice that the saddle-point value $\bar{a}_\mu$ enters the mean-field theory, and thus the response mean-field Hamiltonian with probing field A^s is given as

$$\begin{aligned}H_{\rm mf}(A^s,\bar{a}) = &\sum_{m,ij}\left(t_{m,ij}e^{i\bar{a}_{ij}+iq_m A_{ij}^s}f_{m,i}^\dagger f_{m,j} + \text{H.c.}\right)\\ &+\sum_i \bar{a}_0(N_i - 1), \qquad (6)\end{aligned}$$

where $\bar{a}_\mu$ is a function of A_μ^s as given in (5). Physical quantities of the spin system can be measured from the Gutzwiller-projected ground state of the above mean-field Hamiltonian.

III. GUTZWILLER CONSTRUCTION AND EFFECTIVE-FIELD THEORY

A. Construction of Gutzwiller wave functions

From the fermionic parton representation of $S = 1$ spin operators, one can construct trial spin-wave functions for interacting spin-1 systems via Gutzwiller projection [49],

$$|\psi\rangle_{\rm spin} = P_G|\text{MF}\rangle,$$

where $|\text{MF}\rangle$ is the ground state of the mean-field Hamiltonian (1) and the Gutzwiller-projection operator P_G means only keeping the components of the mean-field state that satisfy the particle-number constraint $\hat{N}_i = 1$. Since the mean-field state suffers from gauge fluctuations, Gutzwiller projection is a simple way to partially integrate out the gauge fluctuations to obtain trial spin-wave functions. For example, in 1D Gutzwiller-projected $SO(3)$, symmetric p-wave weak pairing states belong to a nontrivial SPT phase—the Haldane phase [46].

The above GWFs have two $U(1)$ spin symmetries: one generated by $\sum_i S_{z,i}$ and another by $\sum_i (S_{z,i})^2$. The projected states could be a topologically ordered state enriched by the $U(1)\times U(1)$ symmetry, or a SPT state protected by the $U(1)\times U(1)$ symmetry.

B. Effective theory for projected states

In Sec. II, we have obtained the effective Chern-Simons field theory for the spin system from the mean-field theory, based on hydrodynamical approximation and by dropping higher-order terms in a_μ. In this section, we will use a different approximation to calculate the effective-field theory from Gutzwiller-projected states. Here we make much fewer approximations except assuming that the GWFs can approach very close to the true ground states. We will show that the two approximations produce the same result.

Gutzwiller projection is equivalent to integrating out the temporal component of the internal gauge field, which result in $\delta(\sum_m f_m^\dagger f_m - 1)$. However, the spatial component of the internal gauge fluctuations are not completely "integrated out." Thus, the gauge twisted-boundary angles [50] (or the gauge fluxes through the holes of the torus) $\boldsymbol{\theta} = (\theta_x,\theta_y) = (\oint \tilde{\boldsymbol{a}}\cdot d\boldsymbol{l}_x, \oint \tilde{\boldsymbol{a}}\cdot d\boldsymbol{l}_y)$ can be seen as trial parameters of the GWF and should be "integrated" by hand. To this end, we should know the effective Lagrangian $L_{\text{eff}}(\theta_x,\theta_y)$, which is given as

$$L_{\text{eff}}(\boldsymbol{\theta}) = \langle P_G\psi_{\mathcal{C}}(\boldsymbol{\theta})|\partial_\tau|P_G\psi_{\mathcal{C}}(\boldsymbol{\theta})\rangle + \langle P_G\psi_{\mathcal{C}}(\boldsymbol{\theta})|H|P_G\psi_{\mathcal{C}}(\boldsymbol{\theta})\rangle, \tag{7}$$

where τ is the imaginary time and $|P_G\psi_{\mathcal{C}}(\boldsymbol{\theta})\rangle$ is the projected mean-field state with Chern numbers $\mathcal{C} = (\mathcal{C}_1,\mathcal{C}_0,\mathcal{C}_{-1})$ and gauge twisted-boundary angles $\boldsymbol{\theta}$.

The dynamical term $\langle P_G\psi_{\mathcal{C}}(\boldsymbol{\theta})|H|P_G\psi_{\mathcal{C}}(\boldsymbol{\theta})\rangle$ is expected to be small and will be dropped in the following discussion. The consequence of the dynamic term will be discussed in Sec. IV B. The topological term $\langle P_G\psi_{\mathcal{C}}(\boldsymbol{\theta})|\partial_\tau|P_G\psi_{\mathcal{C}}(\boldsymbol{\theta})\rangle$ is the Berry phase of Gutzwiller-projected states,

$$e^{i\oint \boldsymbol{\mathcal{A}}(\boldsymbol{\theta})\cdot d\boldsymbol{\theta}} = \exp\{\oint \langle P_G\psi_{\mathcal{C}}(\boldsymbol{\theta})|\partial_\tau|P_G\psi_{\mathcal{C}}(\boldsymbol{\theta})\rangle d\tau\} \approx \prod \langle P_G\psi_{\mathcal{C}}(\boldsymbol{\theta})|P_G\psi_{\mathcal{C}}(\boldsymbol{\theta}+\delta\boldsymbol{\theta})\rangle.$$

The Berry connection $\boldsymbol{\mathcal{A}}(\boldsymbol{\theta}) = -i\ln\langle P_G\psi_{\mathcal{C}}(\boldsymbol{\theta})|P_G\psi_{\mathcal{C}}(\boldsymbol{\theta}+\delta\boldsymbol{\theta})\rangle$ (not to be confused with the symmetry connection $\boldsymbol{A}^s$) can be obtained from the wave-function overlap (see Appendix B). Then we can calculate the Berry curvature $\mathcal{F}(\boldsymbol{\theta}) = \partial_{\theta_x}\mathcal{A}_y - \partial_{\theta_y}\mathcal{A}_x$ and the Chern number on the torus formed by the gauge twisted-boundary angles,

$$k = \frac{1}{2\pi}\oint_B d\boldsymbol{\theta}\cdot\boldsymbol{\mathcal{A}}(\boldsymbol{\theta}) = \frac{1}{2\pi}\iint_{\text{torus}} d\theta_x d\theta_y \mathcal{F}(\boldsymbol{\theta}), \tag{8}$$

where B is a big loop that encloses the total area of the torus. It turns out that the Berry curvature is uniform on the (θ_x,θ_y) torus. If we treat (θ_x,θ_y) as the coordinates of a single particle on a torus, then the Berry curvature is the magnetic field that couples to the particle, and $L_{\text{eff}}(\boldsymbol{\theta})$ can be written as

$$L_{\text{eff}}(\boldsymbol{\theta}) = i\frac{k}{2\pi}\dot{\theta}_x\theta_y, \tag{9}$$

where $2\pi k$ is the strength of the "magnetic field" and the dot means ∂_τ. From above Lagrangian, it can be shown (see Appendix C 1) that the ground-state degeneracy of the system is equal to k.

The Hall conductance can be measured by coupling the system to a symmetry flux, or symmetry twisted angles $\boldsymbol{\phi}^s = (\phi_x^s,\phi_y^s) = (\oint \boldsymbol{A}^s\cdot d\boldsymbol{l}_x, \oint \boldsymbol{A}^s\cdot d\boldsymbol{l}_y)$. Now the GWF depends on both $\boldsymbol{\theta}$ and $\boldsymbol{\phi}^s$. The effective Lagrangian is given by $L_{\text{eff}}(\boldsymbol{\theta},\boldsymbol{\phi}^s) \approx \langle P_G\psi_{\mathcal{C}}(\boldsymbol{\theta},\boldsymbol{\phi}^s)|\partial_\tau|P_G\psi_{\mathcal{C}}(\boldsymbol{\theta},\boldsymbol{\phi}^s)\rangle$. Similar to the previous discussion, the effective Lagrangian can also be written as

$$L_{\text{eff}}(\boldsymbol{\theta},\boldsymbol{\phi}^s) = \frac{i}{2\pi}\sum_m \mathcal{C}_m\left(\dot{\theta}_x + q^m\dot{\phi}_x^s\right)\left(\theta_y + q^m\phi_y^s\right).$$

The angles $\boldsymbol{\theta}$ are fluctuating and we should integrate it by hand. Rewriting $\boldsymbol{\theta} = \bar{\boldsymbol{\theta}} + \delta\boldsymbol{\theta}$, where

$$\bar{\boldsymbol{\theta}} = -\frac{\sum_m \mathcal{C}_m q_m}{\sum_m \mathcal{C}_m}\boldsymbol{\phi}^s \tag{10}$$

is obtained from $\frac{\delta L_{\text{eff}}}{\delta\theta_i} = 0$, we then have

$$L_{\text{eff}}(\boldsymbol{\theta},\boldsymbol{\phi}^s) = \frac{i}{2\pi}\sum_m \mathcal{C}_m\left(\tilde{q}_m^2\dot{\phi}_x^s\phi_y^s + \delta\dot{\theta}_x\delta\theta_y\right),$$

where $\tilde{q}_m$ is defined previously. The first term in the bracket gives the physical response $\sigma_H^s = \frac{1}{2\pi}\sum_m \mathcal{C}_m\tilde{q}_m^2$ and the second term indicates the ground-state degeneracy $k = \sum_m \mathcal{C}_m$ (see Appendix C 1).

The Hall conductance can be calculated from the Chern number. When adiabatically varying the symmetry fluxes $\boldsymbol{\phi}^s$, we obtain the Berry phase

$$e^{i\boldsymbol{\mathcal{A}}(\boldsymbol{\phi}^s)\delta\boldsymbol{\phi}^s} = \langle P_G\psi_{\mathcal{C}}(\boldsymbol{\phi}^s,\bar{\boldsymbol{\theta}})|P_G\psi_{\mathcal{C}}(\boldsymbol{\phi}^s+\delta\boldsymbol{\phi}^s,\bar{\boldsymbol{\theta}}+\delta\bar{\boldsymbol{\theta}})\rangle.$$

Integration of the Berry curvature $\mathcal{F}(\boldsymbol{\phi}^s) = \partial_{\boldsymbol{\phi}_x^s}\mathcal{A}_y - \partial_{\boldsymbol{\phi}_y^s}\mathcal{A}_x$ on the (ϕ_x^s,ϕ_y^s) torus gives the Hall conductance,

$$2\pi\sigma_{\text{H}} = \oint_B d\boldsymbol{\phi}^s\cdot\mathcal{A}(\boldsymbol{\phi}^s) = \iint_{\text{torus}} d\phi_x^s d\phi_y^s \mathcal{F}(\boldsymbol{\phi}^s). \tag{11}$$

The internal background gauge flux $\bar{\theta}$ in the above discussion [or $\bar{a}_\mu$ in (5)] is very important. Without $\bar{\theta}$ (or $\bar{a}_\mu$), GWF will give incorrect responses. To see why $\bar{\theta}$ (or $\bar{a}_\mu$) is important, we consider the electromagnetic response as an example. It is known that a spin system is a Mott insulator having no charge response. However, if we barely couple the electromagnetic field A_μ^c to the fermions, then after the Gutzwiller projection the GWF still has dependence on $\boldsymbol{\phi}^c$ (or A_μ^c), and the Chern number for the GWF on the twisted-boundary-angle torus formed by $\boldsymbol{\phi}^c$ is nonzero. This seems to indicate that the system still have electromagnetic quantum Hall effect. This is obviously wrong. To obtain the correct response, we need to couple both A_μ^c and $\bar{a}_\mu$ to the fermions. Since $q^c = (1,1,1)^T$, from (10), $\bar{\boldsymbol{\theta}} = -\boldsymbol{\phi}^c$ (or $\bar{a}_\mu = -A_\mu^c$), so the mean-field state and the projected state are independent on $\boldsymbol{\phi}^c$ (or A_μ^c), which is consistent with the fact that the system is an insulator.

IV. NUMERICAL RESULTS

In this section, we present our numerical results. We will focus on the physical properties of the state $P_G|1-11\rangle$, from which we can judge whether or not it is a SPT state. As a

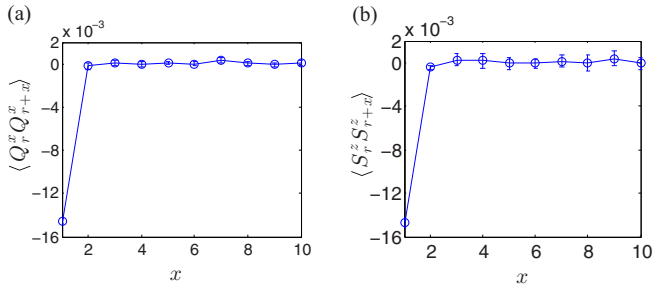

FIG. 2. (Color online) The correlation length on the bulk is extremely short, indicating the bulk is gapped and has no symmetry breaking.

comparison, the chiral spin-liquid (CSL) state $P_G|111\rangle$, which carries intrinsic topological order, is also studied.

A. Short-range correlation in the bulk

We first check that the bulk is gapped without symmetry breaking. To this end, we calculate the spin-spin correlation $\langle S_r^z S_{r+x}^z \rangle$ and quadrupole-quadrupole correlation $\langle Q_r^x Q_{r+x}^x \rangle$, where $Q^x = S_x^2 - S_y^2$. As shown in Fig. 2, the correlations are weak and extremely short ranged (about 2 lattice constants). This indicates that the bulk has a finite excitation gap and no symmetry breaking (otherwise the correlation will be long ranged).

B. Trivial topological order

Here we check if the state $P_G|1-11\rangle$ has topological order by calculating its topological entanglement entropy (TEE) and ground-state degeneracy.

Using the Monte Carlo method, we can obtain the TEE from the second Renyi entropy $S^{(2)} = -\mathrm{Tr}\rho_A^2$ [51–55], where ρ_A is the reduced density matrix of a subsystem A. For topologically ordered states, the entanglement entropy have an universal correction to the area law,

$$S^{(2)} = \alpha \mathbb{A} - \gamma,$$

where $\mathbb{A}$ is the area of the boundary of the subsystem A, and γ is called the topological entanglement entropy. If $P_G|1-11\rangle$ is a SPT state (which is short-range entangled), its TEE γ should be zero.

This is checked numerically. We consider a torus and cut it along the x direction to divide it into two pieces, where each piece contains two noncontractable boundaries see Fig. 3(b). Area law suggests that the second Renyi entanglement entropy is proportional to the circumference of the cut (L_x). In Fig. 3(c), we fix $L_y = 10$ and plot the entropy with L_x. The TEE is given by the intersect, which is very close to 0. The inset shows the dependence of the TEE γ on L_y. The result is that γ exponentially decays to 0 with increasing L_y. The vanishing TEE implies that the state $P_G|1-11\rangle$ is indeed topologically trivial.

The trivial topological order carried by $P_G|1-11\rangle$ can also be reflected by its nondegeneracy on torus. The ground-state degeneracy k can be obtained through (8). Our numerical result shows that the Chern number of $P_G|1-11\rangle$ is 1, while the

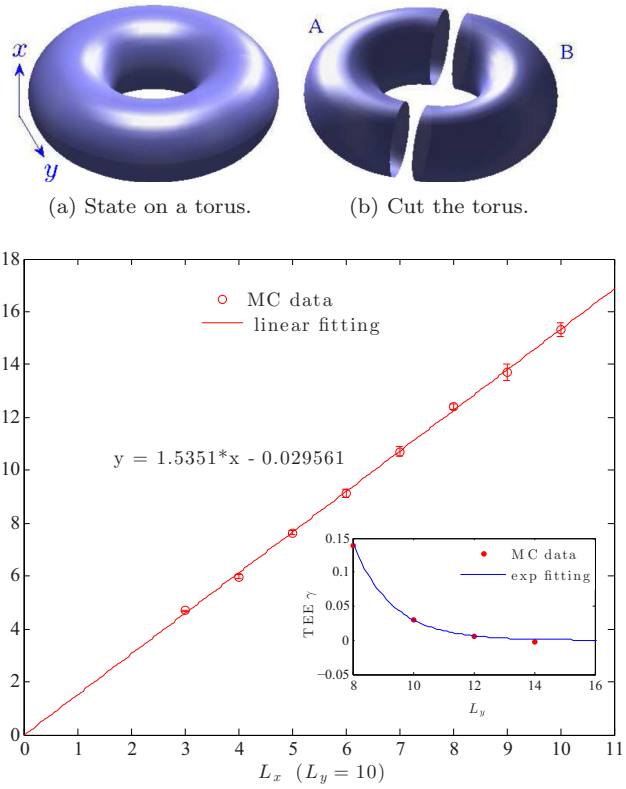

FIG. 3. (Color online) Calculation of topological entanglement entropy (TEE) of state $P_G|1-11\rangle$ on a torus. (a) The geometry of the torus. (b) How the torus is cut into the "system" A and the "environment" B. (c) The second Renyi entanglement entropy $S^{(2)} = -\mathrm{Tr}\rho_A^2$ is plotted vs the circumference L_x. The intercept is the TEE γ. The inset shows that γ exponentially decays to 0 with increasing "length" L_y.

Chern number for the CSL state $P_G|111\rangle$ is 3, in agreement with theoretical prediction $k = \sum_m \mathcal{C}_m$.

To verify that the ground-state degeneracy is indeed equal to k, we calculate the density matrix of projected states with different twisted-boundary angles,

$$\rho(\boldsymbol{\theta}, \boldsymbol{\theta}') = \langle P_G \psi_{\mathcal{C}}(\boldsymbol{\theta}) | P_G \psi_{\mathcal{C}}(\boldsymbol{\theta}') \rangle. \quad (12)$$

The eigenstates of the above density matrix are the orthogonal bases of the Hilbert space spanned by the projected states. In numerical calculation, the torus formed by $\theta_x \in [0, 2\pi)$ and $\theta_y \in [0, 2\pi)$ is discretized into $N \times N$ grids. The eigenvalues of ρ are proportional to the weights of the corresponding eigenstates in the GWF space. We can normalize the total weight to 1. Our data in Fig. 4 show that the total weight is dominated by the first few states, and this result is independent of the system size and the number of grids on the (θ_x, θ_y) torus.

If a dynamic term $\frac{1}{g^2}(\dot{\theta}_x^2 + \dot{\theta}_y^2)$ (where g is a nonuniversal coupling constant determining the internal gauge "photon" gap) is added to Eq. (9), then it describes a single particle moving on a torus in an uniform magnetic field with strength $2\pi k$ [1]. The eigenstates are Landau levels and the lowest Landau level corresponds to the ground state of the spin system. When $g \to \infty$, the gap is infinitely large and only the ground states remain. Generally, g is finite and excited

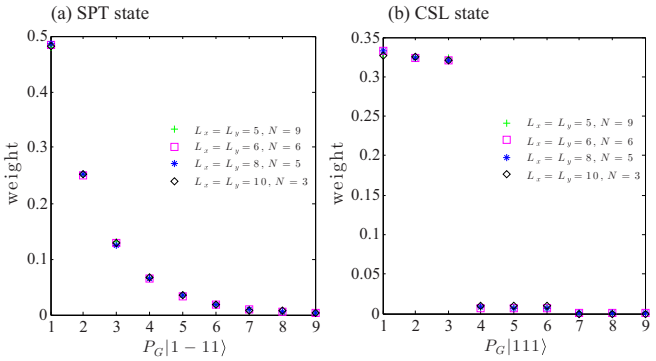

FIG. 4. (Color online) The largest nine (normalized) eigenvalues of the density matrix ρ are shown, which almost exhaust the total weight 1. (a) Data for $P_G|1-11\rangle$; (b) data for $P_G|111\rangle$. The results are almost independent of the system size L_x, L_y (the number of sites is equal to $L_x \times L_y \times 3$) and the number of grids $N \times N$ by which the torus is discretized.

states occur in the GWF space with a weight $\propto e^{-\beta\varepsilon_i}$, where β is a constant and ε_i is the energy of the ith excited state (i.e., the ith Landau level). This is the reason why there are some small weight eigenvalues appearing in Fig. 4. Furthermore, the degeneracy of eigenvalues of ρ reflects the degeneracy of the Landau levels, namely, the degeneracy of eigenstates of the spin system on a torus. From Fig. 4(b), we can learn that all the eigenvalues of ρ for $P_G|111\rangle$ are threefold degenerate (within tolerable error), so the ground state is threefold degenerate. However, for the state $P_G|1-11\rangle$, all the eigenvalues of ρ are nondegenerate, indicating that the ground state is unique.

C. Even-quantized Hall conductance

We adopt Laughlin's gauge-invariant argument on a cylinder to measure the Hall conductances. To this end, we adiabatically insert a $U(1)$ symmetry flux quanta ϕ^s into the cylinder and detect the $U(1)$ symmetry charge pumped from the bottom boundary to the top boundary. Since there are two $U(1)$ symmetries, we measure the Hall conductance, respectively. During the measurement, we used the response mean-field Hamiltonian (6) to obtain the GWFs. Our numerical results of $\sigma_H^{S_z}$ and $\sigma_H^{S_z^2}$ are shown in Fig. 5 and the crossed Hall conductance $\sigma_H^{S_z S_z^2}$ is zero. All of the Hall conductances are even integers, consistent with Chern-Simons theory predictions.

The spin Hall conductance can also be calculated by measuring the Chern number [see Eq. (11)] of the projected states in the torus formed by the $U(1)$ symmetry twisted-boundary angles. Our numerical results confirm the spin Hall conductance shown in Fig. 5.

As mentioned, the spin-spin correlation function in the bulk is short ranged and boring. But the boundary is nontrivial. The nonzero Hall conductance indicates that the boundary should be gapless and the correlation function should be power-law decaying. We would like to directly confirm the power-law behavior for the boundary states. We calculate the correlation function $\langle Q^x(r)Q^x(r+x)\rangle$ (where $Q^x = S_x^2 - S_y^2$) on the boundary (along the x direction) of a cylinder of 300 sites. The cylinder has $L_x \times L_y = 20 \times 5 = 100$ unit cells and is periodic in the x direction and open in the y direction [see

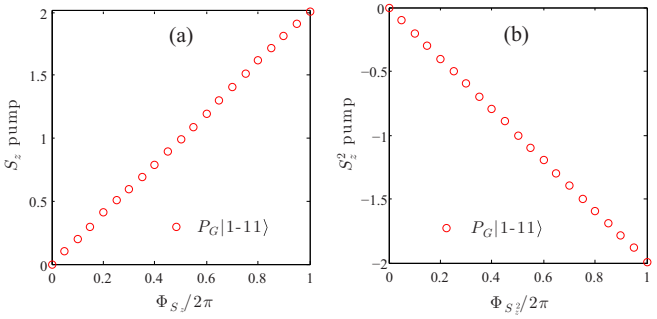

FIG. 5. (Color online) Symmetry charge pumping caused by inserting symmetry fluxes. The Hall conductance is equal to the charge pump by a flux quanta. (a) For the first $U(1)$ symmetry, the Hall conductance is equal to $\frac{1}{2\pi}2$. (b) For the second $U(1)$ symmetry, the Hall conductance is equal to $-\frac{1}{2\pi}2$.

Fig. 1(b)]. The result shows perfect power (see Fig. 6),

$$\langle Q^x(r)Q^x(r+x)\rangle \sim x^{-2.036},$$

and the decaying power -2.036 agrees well with conformal field theory prediction -2 (see Appendix C 2). It should be noted that the correlation function is very small even on the boundary. This may be due to the extremely short correlation length on the bulk.

To completely confirm that $P_G|1-11\rangle$ is a SPT state, we finally need to show that its boundary state is nonchiral, namely, the gapless boundary excitations can be gapped out by symmetry-breaking perturbations. Before projection, the mean-field state $|1-11\rangle$ is obviously chiral and its boundary cannot be gapped out by small local perturbations. To show that the projected state $P_G|1-11\rangle$ is nonchiral, we calculate the boundary correlation function after adding some symmetry-breaking perturbation.

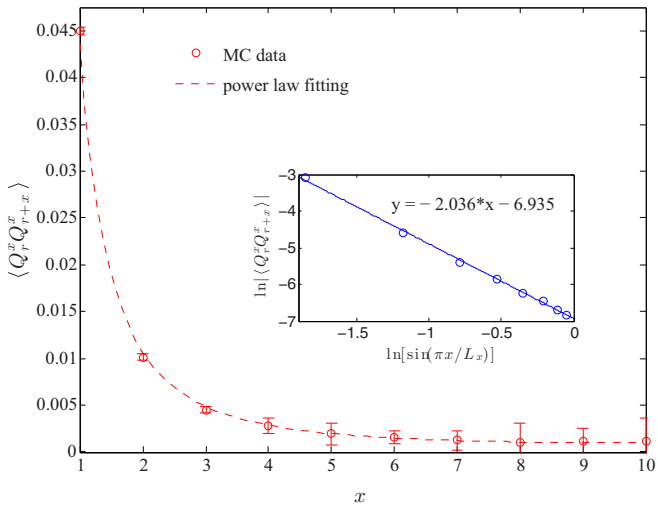

FIG. 6. (Color online) Power-law decaying correlation function on the boundary [the upper boundary of Figs. 1(a)–1(c)] shows that the edge states are gapless. Inset: Log-log fitting. The horizontal axis is set as $\ln(\sin\frac{\pi x}{L_x})$ because of the finite-size effect.

D. Symmetry-protected gapless boundary states

The $U(1)$ symmetry-breaking perturbation that we consider is the following fermion pairing term:

$$H'_{\rm mf} = \Delta^1_{ij} c^\dagger_{1i} c^\dagger_{1j} + \Delta^2_{ij} c^\dagger_{-1i} c^\dagger_{0j} + \text{H.c.} \tag{13}$$

The spin interaction that supports this perturbation might be

$$H' = -(c^\dagger_{1i} c^\dagger_{1j} c_{-1j} c_{0i} + \text{H.c.}) = -(P^x_i Q^x_j - P^y_i Q^y_j),$$

where $P^x = \frac{1}{\sqrt{2}}(S_x S_z + S_z S_x + S_x S_y) = \begin{pmatrix} 0 & 1 & 0 \\ 1 & 0 & 0 \\ 0 & 0 & 0 \end{pmatrix}$, $P^y = \frac{1}{\sqrt{2}}(S_y S_z + S_z S_y + S_y) = \begin{pmatrix} 0 & -i & 0 \\ i & 0 & 0 \\ 0 & 0 & 0 \end{pmatrix}$, and $Q^x = S_x^2 - S_y^2 = \begin{pmatrix} 0 & 0 & 1 \\ 0 & 0 & 0 \\ 1 & 0 & 0 \end{pmatrix}$, $Q^y = S_x S_y + S_y S_x = \begin{pmatrix} 0 & 0 & -i \\ 0 & 0 & 0 \\ i & 0 & 0 \end{pmatrix}$. Similar to S^x, S^y, S^z, the three operators Q^x, Q^y, S^z also form $SU(2)$ algebra.

Our numerical result is shown in Fig. 7, where the correlation functions $\langle S^z_r S^z_{r+x}\rangle$ and $\langle Q^x_r Q^x_{r+x}\rangle$ are both exponentially decaying, as expected.

We also calculate the boundary correlation function of the CSL undergoing the same perturbation. The results in Fig. 8 show that the boundary remains gapless under the perturbation. This comparison give strong evidence that the boundary of the state $P_G|1-11\rangle$ is nonchiral while the CSL state $P_G|111\rangle$ is chiral, as predicted by Chern-Simons theory (see Appendix C 2).

V. CONCLUSION AND DISCUSSION

In summary, using the Monte Carlo method we studied the physical properties of Gutzwiller-projected wave functions. We especially studied the state $P_G|1-11\rangle$ (where $1, -1, 1$ are the mean-field Chern numbers of the fermions f_1, f_0, f_{-1}, respectively), including its spin Hall conductance, correlation function of the gapless edge states, ground-state degeneracy and topological entanglement entropy, and nonrobustness of the gapless edge states. All of this evidence shows that $P_G|1-11\rangle$ is a $U(1) \times U(1)$ symmetry-protected topological state. Our work may shed some light on simple lattice models and experimental realization of SPT phases.

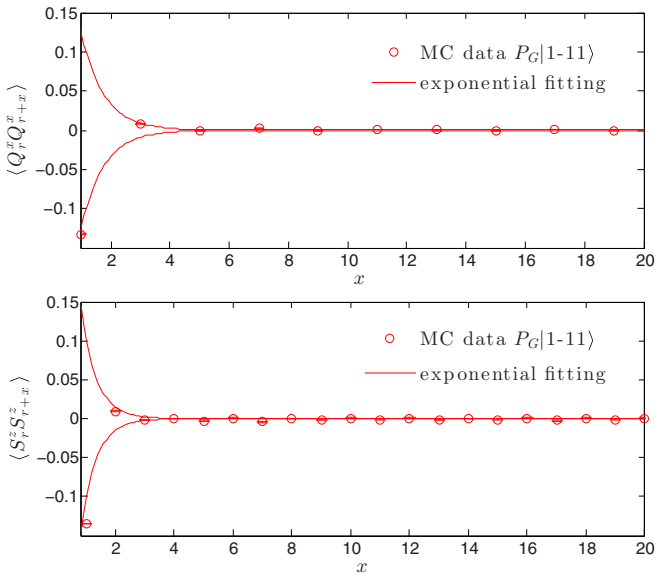

FIG. 7. (Color online) Boundary of SPT phase can be gapped when symmetry is explicitly broken.

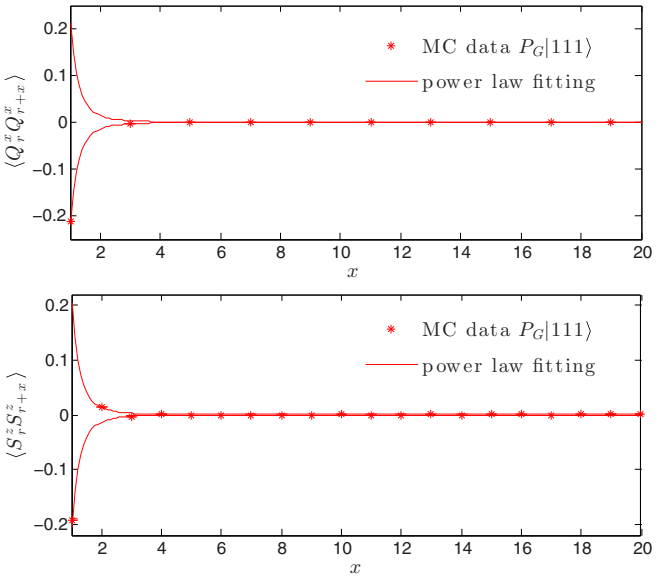

FIG. 8. (Color online) Boundary of CSL phase is robust against all perturbations.

The spin Hall conductance is calculated by measuring the spin pump in the Gutzwiller wave function caused by inserting symmetry flux through the cylinder to the mean-field Hamiltonian. We find that the internal gauge field plays an important role since external symmetry flux will induce a nonzero background internal gauge flux (see also Ref. [40]). Our observation indicates that in general the internal gauge field cannot be ignored in studying the physical response of Gutzwiller-projected wave functions.

We also compared the SPT state $P_G|1-11\rangle$ with the topologically ordered chiral spin-liquid state $P_G|111\rangle$ whose gapless boundary excitations are robust against all local perturbations. Our data imply that the boundary of the SPT state is nonchiral, while the boundary of the chiral spin liquid is chiral. Noticing that at the mean-field level both $|1-11\rangle$ and $|111\rangle$ are chiral, it is remarkable that after Gutzwiller projection (or due to strong interactions), the former becomes nonchiral. This indicates that the physical properties of some mean-field states might be dramatically changed after Gutzwiller projection.

Our Gutzwiller approach can be applied to study SPT states protected by other symmetry groups, such as $SU(2)$ or $SO(3)$ symmetry, and so on. It can also be used to study symmetry-enriched topological phases, where symmetry interplays with topological order resulting in an enriched phase diagram.

Finally, we give some remarks about the Hamiltonians of the Gutzwiller-projected states that we constructed above. In principle, for each Gutzwiller wave function, one can always find a parent Hamiltonian of which the Gutzwiller wave function is the ground state. However, that Hamiltonian is generally very complicated and is difficult to identify.

Nevertheless, approximate Hamiltonians can be constructed. For instance, in Ref. [37], a spin Hamiltonian containing three-body interactions was proposed via perturbation to onsite Hubbard interactions. On the other hand, the reduced density matrix method introduced in Ref. [40] also provides some hint of possible interactions that may stabilize the Gutzwiller wave functions.

ACKNOWLEDGMENTS

We thank Y.-M. Lu, Y. Zhang, Z.-C. Gu, H. Yao, H.-H. Tu, M. Cheng, X.-L. Qi, C. Xu, and P. A. Lee for helpful discussions. We acknowledge the computational time in the cluster of IAS in Tsinghua University. This research is supported in part by Perimeter Institute for Theoretical Physics. Research at Perimeter Institute is supported by the Government of Canada through Industry Canada and by the Province of Ontario through the Ministry of Economic Development & Innovation. Z.X.L. is thankful for the support from NSFC Grant No. 11204149 and the Tsinghua University Initiative Scientific Research Program. X.G.W. is also supported by NSF Grant No. DMR-1005541 and NSFC Grant No. 11274192, and the John Templeton Foundation Grant No. 39901.

APPENDIX A: TOPOLOGICAL ENTANGLEMENT ENTROPY

In Refs. [51–55], several tricks has been introduced to calculate Renyi entropy. The main trick is the "sign trick," which separates the calculation of the magnitude and phase of the swap operator,

$$\begin{aligned} e^{-S_2} &= \langle \mathrm{SWAP} \rangle = \sum_{\alpha_1\alpha_2} \rho_{\alpha_1}\rho_{\alpha_2} \frac{\phi_{\beta_1}\phi_{\beta_2}}{\phi_{\alpha_1}\phi_{\alpha_2}} \\ &= \langle \mathrm{SWAP} \rangle_{\mathrm{amp}} \langle \mathrm{SWAP} \rangle_{\mathrm{phs}}, \end{aligned} \tag{A1}$$

where α_1,α_2 are the spin configurations of two independent systems of the same size, β_1,β_2 are the spin configurations after the swapping of the spins in the holes, and

$$\langle \mathrm{SWAP} \rangle_{\mathrm{phs}} = \sum_{\alpha_1\alpha_2} \tilde{\rho}_{\alpha_1,\alpha_2} e^{i\phi}, \tag{A2}$$

with $\phi = \mathrm{Arg}(\phi^*_{\alpha_1}\phi^*_{\alpha_2}\phi_{\beta_1}\phi_{\beta_2})$ and $\tilde{\rho}_{\alpha_1,\alpha_2} = \frac{|\phi^*_{\alpha_1}\phi^*_{\alpha_2}\phi_{\beta_1}\phi_{\beta_2}|}{\langle \mathrm{SWAP} \rangle_{\mathrm{amp}}}$,

$$\begin{aligned} \langle \mathrm{SWAP} \rangle_{\mathrm{amp}} &= \sum_{\alpha_1,\alpha_2} |\phi^*_{\alpha_1}\phi^*_{\alpha_2}\phi_{\beta_1}\phi_{\beta_2}| \\ &= \sum_{\alpha_1\alpha_2} \rho_{\alpha_1}\rho_{\alpha_2} \left| \frac{\phi_{\beta_1}\phi_{\beta_2}}{\phi_{\alpha_1}\phi_{\alpha_2}} \right|. \end{aligned} \tag{A3}$$

When calculating the phase part, since both the spin configurations before and after the swapping appear in the sampling weight, the trick of updating the inverse and determinant can be applied in the Monte Carlo steps. However, this trick cannot be applied to the magnitude part since the swapped configuration may have zero weight and ϕ_{β_1}, ϕ_{β_2} may not change continuously. To solve this problem and to decrease the error, here we further use the trick to separate the calculation of the magnitude into two steps; in each step, the matrix inverse and determinant updating techniques can be applied. The main idea is to introduce a weight function $f(\alpha_1,\alpha_2)$,

$$f(\alpha_1,\alpha_2) = \begin{cases} 1 & \text{if} \quad \beta_1,\ \beta_2 \text{ are allowed} \\ 0 & \text{if} \quad \beta_1,\ \beta_2 \text{ are not allowed,} \end{cases} \tag{A4}$$

such that

$$\begin{aligned} \langle \mathrm{SWAP} \rangle_{\mathrm{amp}} &= \sum_{\alpha_1\alpha_2} f(\alpha_1,\alpha_2)\rho_{\alpha_1}\rho_{\alpha_2} \left| \frac{\phi_{\beta_1}\phi_{\beta_2}}{\phi_{\alpha_1}\phi_{\alpha_2}} \right| \\ &= \sum_{\alpha_1\alpha_2} \rho'(\alpha_1,\alpha_2) \left| \frac{\phi_{\beta_1}\phi_{\beta_2}}{\phi_{\alpha_1}\phi_{\alpha_2}} \right| \langle f(\alpha_1,\alpha_2) \rangle \\ &= \langle \mathrm{SWAP} \rangle'_{\mathrm{amp}} \langle \mathrm{f}(\alpha_1,\alpha_2) \rangle, \end{aligned} \tag{A5}$$

where $\rho'(\alpha_1,\alpha_2) = \frac{f(\alpha_1,\alpha_2)\rho_{\alpha_1}\rho_{\alpha_2}}{\langle f(\alpha_1,\alpha_2) \rangle}$, and

$$\langle f(\alpha_1,\alpha_2) \rangle = \sum_{\alpha_1,\alpha_2} \rho_{\alpha_1}\rho_{\alpha_2} f(\alpha_1,\alpha_2).$$

Since $f(\alpha_1,\alpha_2)$ is a simple function taking values 0 and 1, the fluctuation is reduced considerably compared to $\langle \mathrm{SWAP} \rangle_{\mathrm{amp}}$ itself.

APPENDIX B: OVERLAP OF WAVE FUNCTIONS

Suppose two normalized wave functions $|\psi_1\rangle$ and $|\psi_2\rangle$ are given as

$$|\psi_1\rangle = \sum_\alpha \frac{f_1(\alpha)}{\sqrt{\sum_\beta |f_1(\beta)|^2}} |\alpha\rangle,$$

$$|\psi_2\rangle = \sum_\alpha \frac{f_2(\alpha)}{\sqrt{\sum_\beta |f_2(\beta)|^2}} |\alpha\rangle,$$

where α means a spin configuration. To calculate the overlap between the two states $\langle\psi_1|\psi_2\rangle$, we introduce another normalized wave function $|\psi_0\rangle$ to generate the Monte Carlo sequence,

$$|\psi_0\rangle = \sum_\alpha \frac{h(\alpha)}{\sqrt{\sum_\beta |h(\beta)|^2}} |\alpha\rangle = \sum_\alpha W_\alpha |\alpha\rangle,$$

where $W_\alpha = \frac{h(\alpha)}{\sqrt{\sum_\beta |h(\beta)|^2}}$ is the weight of α.

Now we have

$$\begin{aligned} \langle\psi_1|\psi_2\rangle &= \sum_\alpha \frac{f_1^*(\alpha) f_2(\alpha)}{\sqrt{\sum_\beta |f_1(\beta)|^2 \sum_\gamma |f_2(\gamma)|^2}} \\ &= \sum_\alpha W_\alpha \frac{f_1^*(\alpha) f_2(\alpha)}{h^*(\alpha)h(\alpha)} \frac{\sum_\sigma |h(\sigma)|^2}{\sqrt{\sum_\beta |f_1(\beta)|^2 \sum_\gamma |f_2(\gamma)|^2}} \\ &= \frac{1}{C} \sum_\alpha W_\alpha \frac{f_1^*(\alpha) f_2(\alpha)}{h^*(\alpha)h(\alpha)}, \end{aligned} \tag{B1}$$

where C is a constant,

$$\begin{aligned} C &= \sqrt{\frac{\sum_\beta |f_1(\beta)|^2}{\sum_\sigma |h(\sigma)|^2} \frac{\sum_\gamma |f_2(\gamma)|^2}{\sum_\delta |h(\delta)|^2}} \\ &= \sqrt{\sum_\beta W_\beta \left| \frac{f_1(\beta)}{h(\beta)} \right|^2 \sum_\gamma W_\gamma \left| \frac{f_2(\gamma)}{h(\gamma)} \right|^2}. \end{aligned} \tag{B2}$$

APPENDIX C: GROUND-STATE DEGENERACY AND BOUNDARY THEORY

1. Ground-state degeneracy

If we integrate out the $a_{m\mu}$ fields in the Chern-Simons action (2), we obtain

$$\mathcal{L}_{\text{eff}}(\tilde{a}) = \frac{i}{4\pi} k \varepsilon^{\mu\nu\lambda} \tilde{a}_\mu \partial_\nu \tilde{a}_\lambda, \tag{C1}$$

where $k = \sum_m \mathcal{C}_m$. If we further integrate out the $\tilde{a}_0$ field, we obtain a zero-strength condition,

$$\partial_x \tilde{a}_y - \partial_y \tilde{a}_x = 0.$$

So we can write $\tilde{a}_i = \partial_i \Lambda + \theta_i / L_i$, where L_i is the size along the i direction and θ_i can be interpreted as the angle of twisted-boundary condition for the fermionic spinons, or the gauge flux through the ith hole of the torus. Substituting the above expression into (C1), we get the effective action

$$L_{\text{eff}} = \frac{i}{2\pi} k \dot{\theta}_x \theta_y, \tag{C2}$$

which yields $[\theta_x, \frac{k}{2\pi}\theta_y] = i$. Define operators $T_i = e^{i\theta_i}$, then we have

$$T_x T_y = T_y T_x e^{i\frac{2\pi}{k}}, \tag{C3}$$

which form a Heisenberg algebra.

Noticing $\tilde{a}_0$ is simply the chemical potential λ_i in (1), integrating out $\tilde{a}_0$ results in exactly one fermion per site, which is equivalent to a Gutzwiller projection. Equation (C2) shows that the GWF still has some degrees of freedom, which determines the ground-state degeneracy.

The representation space of the above Heisenberg algebra (C3) is at least k dimensional. Since $\tilde{a}_\mu$ is a gauge degree of freedom for the original spin model, T_x and T_y will not change the spin Hamiltonian, namely, $[T_x, H] = [T_y, H] = 0$. So the Hilbert space of each energy level forms a representation space of the Heisenberg algebra. In other words, all of the energy levels, including the ground state, are at least k-fold degenerate.

The degeneracy of the ground states can be obtained by calculating the Chern number for the Gutzwiller-projected mean-field states. At the mean-field level, θ_x and θ_y are commuting, so we can construct mean-field states with certain values of θ_x, θ_y, noted as $|\psi_{\mathcal{C}}(\theta_x, \theta_y)\rangle$, where $\mathcal{C}$ denotes $(\mathcal{C}_1 \mathcal{C}_0 \mathcal{C}_{-1})$ for short. The topological term (C2) plays its role when $\tilde{a}_0$ is integrated out (or, equivalently, after the Gutzwiller projection). If we interpret the topological term (C2) as the Berry phase of the Gutzwiller-projected state evolving on the (θ_x, θ_y) torus,

$$\frac{i}{2\pi} k \dot{\theta}_x \theta_y = \langle P_G \psi_{\mathcal{C}}(\theta_x, \theta_y) | \partial_\tau | P_G \psi_{\mathcal{C}}(\theta_x, \theta_y) \rangle, \tag{C4}$$

then k corresponds to the Chern number of the projected state,

$$2\pi k = \oint \frac{k}{2\pi} \dot{\theta}_x \theta_y d\tau = \oint_B d\boldsymbol{\theta} \cdot \boldsymbol{\mathcal{A}} \tag{C5}$$

$$= \oint_{\text{torus}} d\theta_x d\theta_y \mathcal{F}(\boldsymbol{\theta}), \tag{C6}$$

where $\boldsymbol{\mathcal{A}} = -i \langle P_G \psi_{\mathcal{C}}(\boldsymbol{\theta}) | \partial_{\boldsymbol{\theta}} | P_G \psi_{\mathcal{C}}(\boldsymbol{\theta}) \rangle$ is the Berry connection [if θ_x, θ_y are discretized, then we have $e^{i\boldsymbol{\mathcal{A}}\cdot\delta\boldsymbol{\theta}} = \langle P_G \psi_{\mathcal{C}}(\boldsymbol{\theta}) | P_G \psi_{\mathcal{C}}(\boldsymbol{\theta} + \delta\boldsymbol{\theta}) \rangle$] and $\mathcal{F}(\boldsymbol{\theta}) = \partial_{\theta_x} \mathcal{A}_y - \partial_{\theta_y} \mathcal{A}_x$ is the Berry curvature; B is the big loop enclosing the total area of the (θ_x, θ_y) torus.

Generally, the projected state $|P_G \psi_{\mathcal{C}}(\theta_x, \theta_y)\rangle$ is not an eigenstate of $T_i = e^{i\theta_i}$. Instead, an eigenstate $|n_i\rangle$ of $T_i |n\rangle_i = e^{i2n\pi/k} |n\rangle_i$ (here, $n = 0, 1, \ldots, k-1$) is a superposition of $|P_G \psi_{\mathcal{C}}(\theta_x, \theta_y)\rangle$,

$$|n\rangle_i = \int d\theta_x d\theta_y \xi_{n_i}(\theta_x, \theta_y) |P_G \psi_{\mathcal{C}}(\theta_x, \theta_y)\rangle, \tag{C7}$$

where $\xi_{n_i}(\theta_x, \theta_y)$ is a weight function in analog to a single-particle wave function in the first Landau level [1].

2. Boundary theory

In the remaining part, we will introduce an equivalent K-matrix description as the low-energy effective theory. Integrating out the internal gauge field $\tilde{a}_\mu$ first, we obtain $\sum_m \partial_\nu a_{m\lambda} = 0$, or $\sum_m a_{m\lambda} = 0$ up to a constant field. Eliminating $a_{0\mu}$, we obtain the low-energy effective Chern-Simons theory for the spin system [37],

$$\mathcal{L} = -\frac{i}{4\pi} \varepsilon^{\mu\nu\lambda} \begin{pmatrix} a_{1\mu} & a_{-1\mu} \end{pmatrix} K \partial_\nu \begin{pmatrix} a_{1\lambda} \\ a_{-1\lambda} \end{pmatrix} + \frac{i}{2\pi} \varepsilon^{\mu\nu\lambda} A^s_\mu \begin{pmatrix} q_1 & q_{-1} \end{pmatrix} \partial_\nu \begin{pmatrix} a_{1\lambda} \\ a_{-1\lambda} \end{pmatrix}, \tag{C8}$$

where $K = \begin{pmatrix} \mathcal{C}_1^{-1} + \mathcal{C}_0^{-1} & \mathcal{C}_0^{-1} \\ \mathcal{C}_0^{-1} & \mathcal{C}_{-1}^{-1} + \mathcal{C}_0^{-1} \end{pmatrix}$, A^s_μ is the probing field according to some symmetry, and $q = \begin{pmatrix} q_1 \\ q_{-1} \end{pmatrix}$ is the "charge vector" coupling to this probe field. For the $\sum_i S^z_i$ conservation symmetry, $q = \begin{pmatrix} 1 \\ -1 \end{pmatrix}$, while for the $\sum_i (S^z_i)^2$ conservation symmetry, $q = \begin{pmatrix} 1 \\ 1 \end{pmatrix}$. The Hall conductance is given by $\sigma_H = \frac{1}{2\pi} q^T K^{-1} q$.

Since (C8) is not gauge invariant if the system has a boundary, we need to introduce a boundary action to recover the gauge invariance,

$$\mathcal{L}_{\text{boundary}} = -\frac{i}{4\pi} K_{IJ} \partial_\tau \phi_I \partial_x \phi_J - V_{IJ} \partial_x \phi_I \partial_x \phi_J, \tag{C9}$$

where $I, J = 1, -1$, and the field ϕ_I only exist on the boundary and is defined such that $a_{I\mu} = \partial_\mu \phi_I$. The ϕ_I field satisfies the Kac-Moody algebra,

$$[\partial_x \phi_I, \partial_y \phi_J] = 2\pi i (K^{-1})_{IJ} \partial_x \delta(x - y). \tag{C10}$$

The fermion operators can be written as $f_1 \sim e^{-i\phi_1}, f_{-1} \sim e^{-i\phi_{-1}}$. The spin-density operator is given as $S_z \sim \partial_x \phi_1 - \partial_x \phi_{-1}$, and

$$Q^{\pm} = \tfrac{1}{2}(Q^x \pm i Q^y) \sim e^{i\phi_{\pm 1} - i\phi_{\mp 1}}. \tag{C11}$$

If $\mathcal{C}_1 = 1, \mathcal{C}_0 = -1, \mathcal{C}_{-1} = 1$, then the K matrix is given as $K = \begin{pmatrix} 0 & -1 \\ -1 & 0 \end{pmatrix}$, and from (C10) and (C11), we obtain the scaling law

$$\langle Q^+(r) Q^-(r + x) \rangle \sim x^{-2},$$

which is verified by the numerical result given in Sec. III.

Furthermore, for the above K matrix, since $l = \begin{pmatrix} n \\ 0 \end{pmatrix}$ or $l = \begin{pmatrix} 0 \\ n \end{pmatrix}$ (n is an integer) satisfies

$$l^T K^{-1} l = 0, \tag{C12}$$

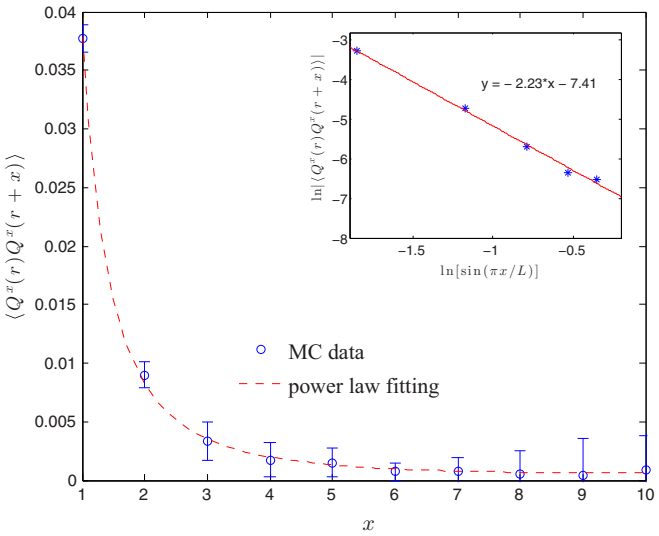

FIG. 9. (Color online) Correlation function of the boundary in an uniform Zeeman field $B_x = 0.4$. Power-law decaying correlation function on the boundary shows that the edge states are still gapless. Inset: Log-log fitting, which shows that the decaying power is approximately -2.23.

the Higgs term [24] that may gap out the boundary is $\cos(n\phi_1)$ or $\cos(n\phi_{-1})$. Equation (C12) is the gapping condition for the perturbations. For instance, the pairing perturbation discussed in Sec. IV D satisfies the gapping condition. On the other hand, if this condition is not satisfied for some perturbation, for example, a Zeeman field coupling

$$H' = B_x S_x \sim \cos(2\phi_1 + \phi_{-1}) + \cos(2\phi_{-1} + \phi_1),$$

which does not contain the Higgs term, then the boundary remains gapless and even the symmetry is explicitly broken. This is verified by our numerical result shown in Fig. 9, where the correlation function $\langle Q^x(r)Q^x(r+x)\rangle$ remains power law if we add a Zeeman field $B_x = 0.4$ (in units of t_{ij}) to the whole system.

Finally, we give the Chern-Simons theory of the CLS state where $\mathcal{C}_1 = \mathcal{C}_0 = \mathcal{C}_{-1} = 1$. Form (C8), the K matrix of the CSL, is given as $K = \left(\begin{smallmatrix} 2 & 1 \\ 1 & 2 \end{smallmatrix}\right)$. Since $\det K = 3$, the ground-state degeneracy of CSL on a torus is 3. Furthermore, since the gapping condition (C12) has no solutions, the boundary cannot be gapped out by small local perturbations.

[1] X. G. Wen, Phys. Rev. B **40**, 7387 (1989).
[2] X. G. Wen and Q. Niu, Phys. Rev. B **41**, 9377 (1990).
[3] X. G. Wen, Int. J. Mod. Phys. B **04**, 239 (1990).
[4] D. C. Tsui, H. L. Stormer, and A. C. Gossard, Phys. Rev. Lett. **48**, 1559 (1982).
[5] R. B. Laughlin, Phys. Rev. Lett. **50**, 1395 (1983).
[6] P. Anderson, Mater. Res. Bull. **8**, 153 (1973).
[7] P. W. Anderson, Science **235**, 1196 (1987).
[8] L. D. Landau, Phys. Z. Sowjetunion **11**, 26 (1937).
[9] V. L. Ginzburg and L. D. Landau, Zh. Eksp. Teor. Fiz. **20**, 1064 (1950).
[10] X. Chen, Z.-C. Gu, and X.-G. Wen, Phys. Rev. B **82**, 155138 (2010).
[11] A. Kitaev and J. Preskill, Phys. Rev. Lett. **96**, 110404 (2006).
[12] M. Levin and X.-G. Wen, Phys. Rev. Lett. **96**, 110405 (2006).
[13] Z.-C. Gu and X.-G. Wen, Phys. Rev. B **80**, 155131 (2009).
[14] F. Pollmann, A. M. Turner, E. Berg, and M. Oshikawa, Phys. Rev. B **81**, 064439 (2010).
[15] F. Haldane, Phys. Lett. A **93**, 464 (1983).
[16] F. D. M. Haldane, Phys. Rev. Lett. **50**, 1153 (1983).
[17] C. L. Kane and E. J. Mele, Phys. Rev. Lett. **95**, 146802 (2005).
[18] B. A. Bernevig and S.-C. Zhang, Phys. Rev. Lett. **96**, 106802 (2006).
[19] J. E. Moore and L. Balents, Phys. Rev. B **75**, 121306 (2007).
[20] L. Fu, C. L. Kane, and E. J. Mele, Phys. Rev. Lett. **98**, 106803 (2007).
[21] X.-L. Qi, T. L. Hughes, and S.-C. Zhang, Phys. Rev. B **78**, 195424 (2008).
[22] X. Chen, Z.-C. Gu, Z.-X. Liu, and X.-G. Wen, Phys. Rev. B **87**, 155114 (2013).
[23] Z. Bi, A. Rasmussen, and C. Xu, arXiv:1309.0515.
[24] Y.-M. Lu and A. Vishwanath, Phys. Rev. B **86**, 125119 (2012).
[25] X. Chen and X.-G. Wen, Phys. Rev. B **86**, 235135 (2012).
[26] T. Senthil and M. Levin, Phys. Rev. Lett. **110**, 046801 (2013).
[27] N. Regnault and T. Senthil, Phys. Rev. B **88**, 161106 (2013).
[28] Z.-X. Liu and X.-G. Wen, Phys. Rev. Lett. **110**, 067205 (2013).
[29] X.-G. Wen, Phys. Rev. B **65**, 165113 (2002).
[30] S.-P. Kou, M. Levin, and X.-G. Wen, Phys. Rev. B **78**, 155134 (2008).
[31] S.-P. Kou and X.-G. Wen, Phys. Rev. B **80**, 224406 (2009).
[32] A. Mesaros and Y. Ran, Phys. Rev. B **87**, 155115 (2013).
[33] L.-Y. Hung and Y. Wan, Phys. Rev. B **87**, 195103 (2013).
[34] Y.-M. Lu and A. Vishwanath, arXiv:1302.2634.
[35] X. Chen, Z.-X. Liu, and X.-G. Wen, Phys. Rev. B **84**, 235141 (2011).
[36] M. Levin and Z.-C. Gu, Phys. Rev. B **86**, 115109 (2012).
[37] Y.-M. Lu and D.-H. Lee, Phys. Rev. B **89**, 184417 (2014).
[38] P. Ye and X.-G. Wen, Phys. Rev. B **87**, 195128 (2013).
[39] Z.-X. Liu, Z.-C. Gu, and X.-G. Wen, arXiv:1404.2818.
[40] J.-W. Mei and X.-G. Wen, arXiv:1407.0869.
[41] S. D. Geraedts and O. I. Motrunich, arXiv:1408.1096.
[42] H.-H. Tu, A. E. Nielsen, and G. Sierra, Nucl. Phys. B **886**, 328 (2014).
[43] P. Lee, N. Nagaosa, and X.-G. Wen, Rev. Mod. Phys. **78**, 17 (2006).
[44] Z.-X. Liu, Y. Zhou, and T.-K. Ng, Phys. Rev. B **82**, 144422 (2010).
[45] Z.-X. Liu, Y. Zhou, and T.-K. Ng, Phys. Rev. B **81**, 224417 (2010).
[46] Z.-X. Liu, Y. Zhou, H.-H. Tu, X.-G. Wen, and T.-K. Ng, Phys. Rev. B **85**, 195144 (2012).

[47] S. Bieri, M. Serbyn, T. Senthil, and P. A. Lee, Phys. Rev. B **86**, 224409 (2012).
[48] $\tilde{J}_0 = 0$ is simply the number constraint, which induces $\tilde{J}_i = 0$.
[49] C. Gros, Ann. Phys. **189**, 53 (1989).
[50] Q. Niu, D. J. Thouless, and Y.-S. Wu, Phys. Rev. B **31**, 3372 (1985).
[51] M. B. Hastings, I. González, A. B. Kallin, and R. G. Melko, Phys. Rev. Lett. **104**, 157201 (2010).
[52] J. I. Cirac and G. Sierra, Phys. Rev. B **81**, 104431 (2010).
[53] Y. Zhang, T. Grover, and A. Vishwanath, Phys. Rev. Lett. **107**, 067202 (2011).
[54] Y. Zhang, T. Grover, and A. Vishwanath, Phys. Rev. B **84**, 075128 (2011).
[55] J. Pei, S. Han, H. Liao, and T. Li, Phys. Rev. B **88**, 125135 (2013).